9.5

Evolution of tornado-like vortices in a numerically simulated supercell thunderstorm

Leigh Orf
Department of Geography, Central Michigan University, Mount Pleasant, Michigan
leigh.orf@cmich.edu

Robert Wilhelmson
Department of Atmospheric Sciences, University of Illinois, Urbana, Illinois

1 Introduction

Recent observational studies of supercell thunderstorms indicate that low-level vertically oriented vortices with diameters 500 m or less may play a crucial role in some cases of tornadogenesis (Bluestein et al. 1997; Bluestein et al. 2003). Cyclonic vortices with a diameter on the order of 100-200 m found along the leading edge of a rear-flank gust front preceded tornadogenesis in an observed supercell (Bluestein et al. 2003). It is likely that rotation on such scales, which is difficult to observe for both technological and logistical reasons, occurs frequently within supercell thunderstorms.

Many three-dimensional numerical modeling studies of supercells are found in the literature and have elucidated many of the features of these storms. However, the vast majority of these simulations have been run at grid spacings on the order of 1 kilometer which is far too coarse to resolve flow on the order of a few hundred meters (Bryan et al. 2003).

In this study, a supercell thunderstorm is simulated using the NCOMMAS model with horizontal grid spacing of 100 meters and a stretched vertical grid with 70 meter spacing near the surface. During the course of the four-hour simulation, numerous cyclonic vorticity features with a horizontal scale on the order of 500 m are found extending upwards from the surface behind the leading edge of the gust front along the storm's right flank. Most of these features originate ahead of and to the left (all directions relative to the storm's motion vector) of the supercell updraft along the leading edge of outflow pulses initiated from precipitation-induced downdrafts. These features typically propagate along and slightly behind the leading edge of the cold pool, moving below the main updraft and continuing along the gust front below the storm's flanking line. Some of these features are associated with vertical vorticity exceeding 0.2 s^{-1}, a drop in central pressure on the order of 5 hPa, and ground-relative surface winds exceeding 35 m s^{-1}.

2 Methodology

This simulation was carried out with NCOMMAS, a three-dimensional nonhydrostatic cloud model with ice microphysics (Wicker and Skamarock 2002). A horizontal grid spacing of 100 meters was chosen on the inner part of the model domain, stretching to 250 m outside of the region centered on the storm. A constant vertical grid spacing of 70 m was used in the bottom six model gridpoints, stretching to 530 m at the top of the model domain. The physical model domain spanned 87.5 by 75.0 by 17.5 km. The model sounding is nearly identical to that of Wilhelmson and Klemp (1981), containing a quarter-circle hodograph with unidirectional shear above 1.1 km AGL and 3500 J kg^{-1} CAPE. The model was initialized with a warm bubble and was integrated for four hours. A carefully chosen box speed (16.8 m s^{-1} eastward and 10.4 m s^{-1} southward) matching storm motion ensured the center of the supercell explored in this simulation remain centered within the 100 m non-stretched inner horizontal grid. Model history files were saved every 5 s model time in order to capture the high temporal resolution of the vorticity features (Bluestein et al.

2003). The microphysics used is that of Gilmore et al. (2004) which is based on that of (Lin et al. 1983). Slope intercept parameters for hail identical to Lin et al. (1983) were chosen (hail density = 900 kg m^{-1}, hail intercept = 4×10^4 m^{-4}) such that the model produces large hail.

3 Findings

3.1 Main supercell characteristics

Fig. 1 contains a panoramic view of a rendering of the storm three hours into the simulation. This storm contains many of the signatures of a classic supercell, exhibiting a long-lived quasi-steady updraft with vertical velocities consistently exceeding 50 $\mathrm{m\,s^{-1}}$ over several kilometers in the vertical at midlevels. The storm contains a well-defined flanking line which for the majority of the simulation is smooth and does not contain discrete cells (Lemon 1976). The storm studied here is the right-mover of a split pair (Wilhelmson and Klemp 1981). A second storm is also present to the northeast of the main cell, forced by surface convergence from the right-mover, similar to Wilhelmson and Klemp (1981).

Fig. 2 is a closeup of isosurfaces of cloud water, rain water, hail, vertical vorticity and cold pool boundary centered near the occlusion point of the forward and rear flank downdrafts. Six low-level vertical vorticity features are apparent, extending from near the occlusion towards the eastern edge of the flanking line. Each of these features contains a vortex-relative circular flow and the features are moving generally from right to left behind the cold pool towards the flanking line. A lowering in the cloud base is also observed beneath these features.

3.2 Low-level vortex features

In general, these vortex features form behind the leading edge of the cold pool where there is significant convergence between cold outflow air and environtmental inflow. The cold outflow from precipitation-induced downdrafts is very unsteady in nature throughout the simulation. Downdraft "pulses" occur occasionally producing what appear to be embedded macrobursts (Fujita 1981). The strongest vortices form along the leading edge of the wall jet outflow of these downbursts. Vortices generally propagate parallel to the gust front and some become situated directly under the main supercell updraft; however the intense vortex stretching required for tornadogenesis does not occur. Some features continue along the gust front and propagate without notable amplification along the flanking line, which, for most of the simulation, is rather smooth in appearance, lacking individual convective cells (see Fig. 1).

In Fig. 3 surface horizontal wind vectors plotted at model grid resolution are shown in addition to surface vertical vorticity, cold pool boundary, and mid-level updraft location. The age of each vortex is generally from youngest to oldest as you move from the upper right to lower left.

The youngest (top) three vortices in Fig. 3 form along a line of convergence at the leading edge of the outflow of a macroburst-like feature which is embedded in the cold pool (see Figs. 8 and 9). The leading edge of this southward-flowing outflow encounters inflow air with a significant westward component, creating a broad region of vorticity exceeding 0.01 s^{-1}. Vortex amplification along this vortex sheet occurs rapidly for one of these features features which reaches a maximum value of ζ of 0.25 s^{-1}

3.2.1 Initiation of an intense vortex feature

Figs. 4–7 chart the origin of the strongest vorticity feature shown in Fig. 3. In Fig. 4, storm-relative surface horizontal winds, rain, hail, and horizontal (ξ) vorticity isosurfaces are shown, along with four ribbon tracers which pass through the downdraft and outflow of the macroburst. At this time the hail-induced downdraft, which forms to the east of the existing precipitation, has not yet formed. Horizontal (ξ) vorticity is located behind the leading edge of the gust front where a classic gust front head circulation is found.

Three minutes later, a shaft of hail and rain has formed to the east, inducing a downdraft (see Fig. 5). This oblong-shaped downdraft consists of a broad swath of winds with typical downdraft velocities of 13 $\mathrm{m\,s^{-1}}$ extending from 600 to 1.5 km AGL, and exhibiting a peak downdraft exceeding 20 $\mathrm{m\,s^{-1}}$ as low as 600 m AGL. Two minutes later a strongly divergent surface wind pattern is seen as the macroburst outflow extends outward (see Fig. 6), and five minutes after the initial downdraft pulse, intense vertical vorticity is occurring at the surface along the southeastern flank of the macroburst outflow (see Figs. 6 and 9). The outflow pulse, which is occurring in a strongly sheared environment, has created a roll-vortex circulation containing horizontal vorticity values exceeding -0.1 s^{-1}, and this vorticity is being tilted by updraft winds found along the leading edge of the roll vortex. Stretching is maximized near the surface below the same updraft. It should be noted that the main supercell updraft is to the south of this feature and is not responsible for the initiation of this vertical vorticity feature.

Figures 8 and 9 provide a surface perspective of the macroburst and its relationship to the initiation of the strongest vortex feature. The northern flank of the main updraft at 2.7 km is indicated by a thick green line in the lower part of the figure (the updraft contours to the right in both figures represent a small, transient updraft and is not evidence of a restructuring of the mesocyclone).

3.3 Elevated vortex features

Figure 10 is a view looking eastward at the main supercell updraft and isosurfaces of the magnitude of the vorticity vector at 2:59:35. A striking feature of this figure is the group of elevated vortices which flank the right and rear flanks of the updraft. These features are very common throughout the simulation. These features begin as horizontal vortices (large positive values of ξ) on the right flank of the updraft. This horizontally oriented vorticity is then tilted by the strong vertical wind gradient across the updraft itself, and becomes oriented with a significant vertical component. These vortices form cyclically and remain elevated, only occasionally interacting with other surface vortex features. Animations of the supercell thunderstorm reaveal the presence of these vortices in a periodic pulsing seen in the updraft, cloud, and precipitation values in their vicinity. The progression of these features would be missed at a coarser temporal sampling of the model data.

4 Discussion

Throughout the course of this simulation, numerous vorticity features are found behind the cold pool. One of the strongest features found in the simulation is initiated along the leading edge of an intense hail-induced forward flank downdraft. This feature is initiated from the tilting of horizontally oriented vorticity along the leading edge of the outflow from this macroburst. The tilting and stretching which initiated this vertical vorticity feature is caused from the updraft along the leading edge of this roll-vortex circulation, and not by the main supercell updraft.

It is suggested that the choice of large hail parameters in the model microphysics produces a forward flank downdraft which is closer to the location of the updraft than is typically considered to occur in a classic supercell (e.g., the plan view of a tornadic supercell diagram found in Lemon and Doswell (1979)), and which may produce more intense downdrafts due to larger hail terminal velocities and increased frictional drag.

One important finding from this work is that cyclonic vertical vorticity features with diameters on the order of 500 m are plentiful throughout a numerical simulation of a supercell at 100 m horizontal grid spacing. In addition, many of these features propagate underneath the main supercell updraft where they are favorably located for initiating tornadogenesis via stretching. These findings are consistent with observations of vorticity evolution during cyclic tornadogenesis (Dowell and Bluestein 2002a; Dowell and Bluestein 2002b). These features appear very similar to the “seeds from which some tornadoes formed” observed using Doppler radar observations of a supercell by Bluestein et al. (1997).

Many of these vortices are long-lived and propagate along the flanking line before dissipating. Tornadoes have been observed to form from shear features within flanking line convection (e.g., Wakimoto and Atkins (1996)) and their presence in this simulation suggests a formation mechanism for these features.

Elevated vortex features are also found flanking the supercell updraft, progressing in a periodic manner. The significance of these features in not yet clear.

5 Future Work

A vorticity budget analysis and Lagrangian parcel analysis for several of the vortex features is being undertaken. Higher-resolution simulations will be run in order to find whether the vortices are being properly resolved and that we are converging to a vortex scale that does not decrease with increasing grid resolution. The sensitivity of vortex initiation with microphysical hail parameters is also warranted due to the importance of strong hail-induced downdrafts.

6 Acknowledgments

This work is supported by Central Michigan University and through NSF Grant ATM-9986672. Numerical simulations were carried out on Central Michi-

gan University's IBM Regatta. Isosurface renderings were produced using the Persistence of Vision Raytracer (PoVRay) and Vis5D, and line drawings were produce using NCAR Graphics.

References

Bluestein, H. B., S. G. Gaddy, D. D. Dowell, A. L. Pazmany, J. C. Galloway, R. E. McIntosh, and H. Stein, 1997: Doppler radar observations of substorm-scale vortices in a supercell. *Mon. Wea. Rev.* **125**, 1046–1059.

Bluestein, H. B., C. C. Weiss, and A. L. Pazmany, 2003: Mobile Doppler radar observations of a tornado in a supercell near Bassett, Nebraska, on 5 June 1999. Part I: Tornadogenesis. *Mon. Wea. Rev.* **131**, 2954–2967.

Bryan, G. H., J. C. Wyngaard, and J. M. Fritsch, 2003: Resolution requirements for the simulation of deep moist convection. *Mon. Wea. Rev.* **131**, 2394–2416.

Dowell, D. C. and H. B. Bluestein, 2002: . The 8 June McLean, Texas, storm. Part I: Observations of cyclic tornadogenesis.

Dowell, D. C. and H. B. Bluestein, 2002: . The 8 June McLean, Texas, storm. Part II: Cyclic tornado formation, maintenance, and dissipation.

Fujita, T. T., 1981: Tornadoes and downbursts in the context of generalized planetary scales. *J. Atmos. Sci.* **58**, 1164–1181.

Gilmore, M. S., J. M. Straka, and E. N. Rasmussen, 2004: Precipitation uncertainty due to variations in precipitation particle parameters within a simple microphysics scheme. *Mon. Wea. Rev.* **In Press**.

Lemon, L. R., 1976: The flanking line, a severe thunderstorm intensification source. *J. Atmos. Sci.* **33**, 686–694.

Lemon, L. R. and C. A. Doswell, 1979: Severe thunderstorm evolution and mesocyclone structure as related to tornadogenesis. *Mon. Wea. Rev.* **107**, 1184–1197.

Lin, Y.-L., R. D. Farley, and H. D. Orville, 1983: Bulk parameterization of the snow field in a cloud model. *J. Climate Apple. Meteor.* **22**, 1065–1092.

Wakimoto, R. M. and N. T. Atkins, 1996: Observations on the origins of rotation: The Newcastle tornado during VORTEX 94. *Mon. Wea. Rev.* **124**, 384–407.

Wicker, L. J. and W. C. Skamarock, 2002: Time-splitting methods for elastic models using forward time schemes. *Mon. Wea. Rev.* **130**, 2088–2097.

Wilhelmson, R. B. and J. B. Klemp, 1981: A three-dimensional numerical simulation of splitting severe storms on 3 April 1964. *J. Atmos. Sci.* **38**, 1581–1600.

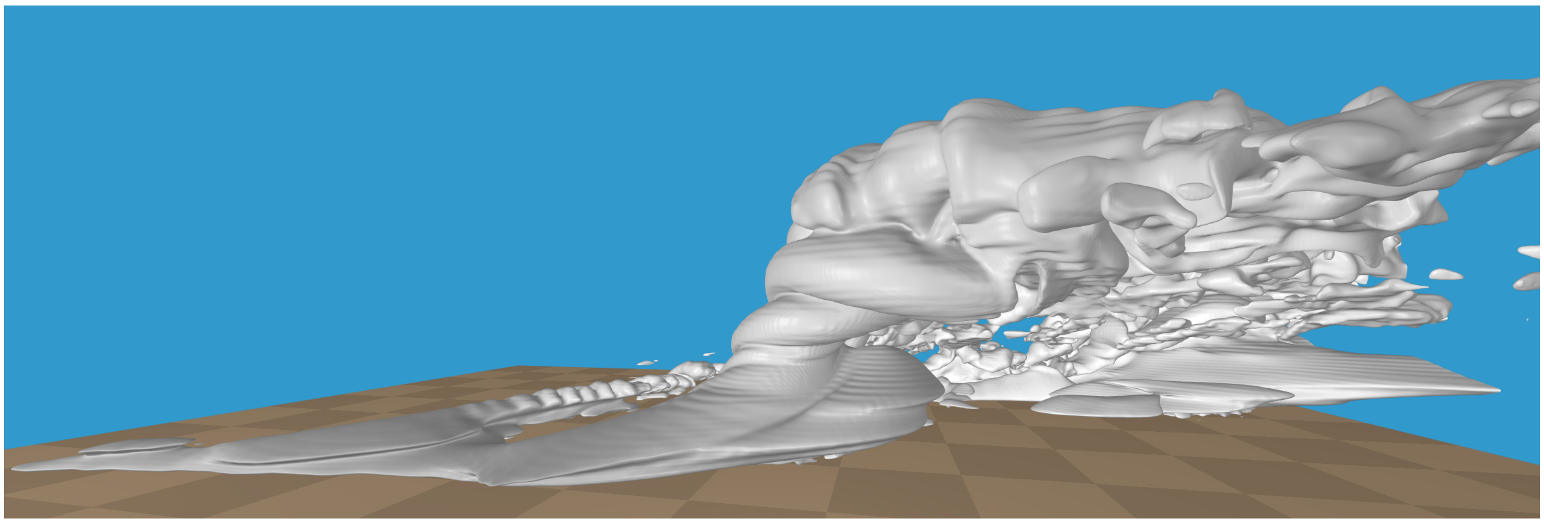

Figure 1: An aerial view of the storm at 3:00:00. The isosurface represents 0.2 g kg^{-1} of the sum of cloud water and ice. Grid squares are 5 km on a side.

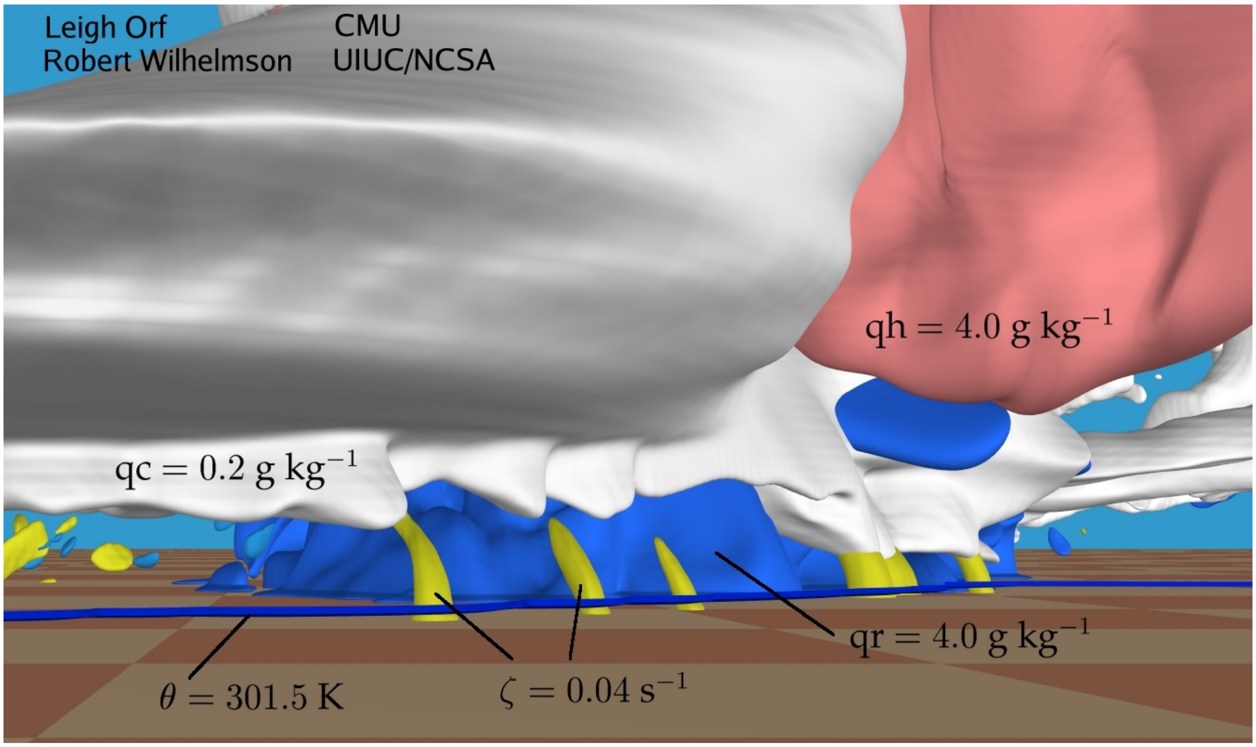

Figure 2: Model state at 2:55:00 (h:mm:ss). Isosurfaces of cloud water, hail, rain, and vertical vorticity are shown, as well as the leading edge of the cold pool. Grid squares are 5 km on a side.

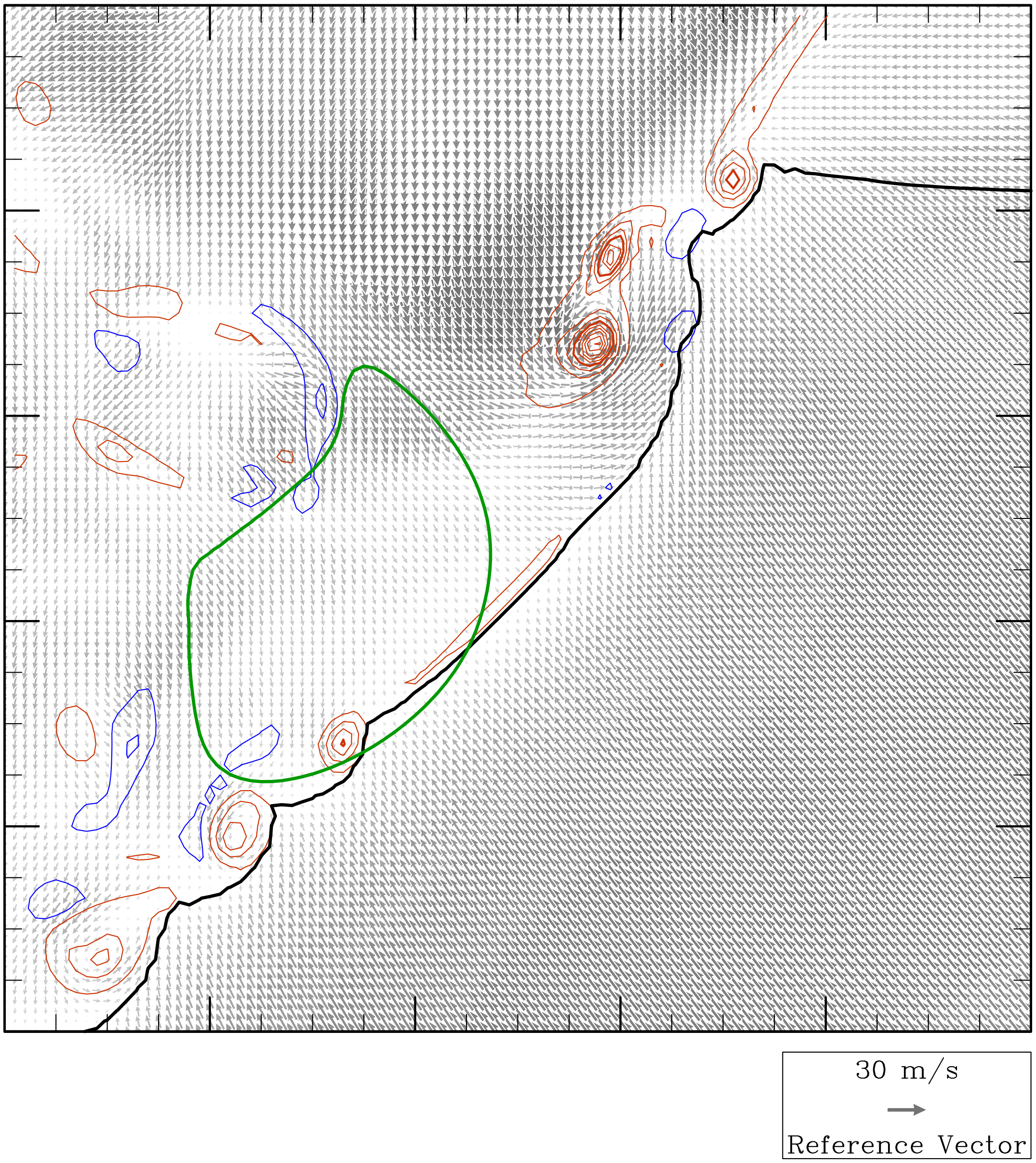

Figure 3: Surface conditions at 2:56:20 including: ζ in 0.03 s^{-1} contour intervals starting at +/-0.01 s^{-1} (positive values in red, negative in blue). The thick black line denotes the leading edge of the cold pool (θ = 301.5 K). The thick green line indicates the location of the updraft (20 m s^{-1} contour at 2.7 km AGL). Surface wind vectors are shown at model grid resolution and are colored by magnitude from light gray (weak winds) to dark gray (strong winds). Surface wind vectors are relative to the strongest vortex (third from the top, ahead of the strongest horizontal winds, which is moving towards the southwest at 5 m s^{-1} relative to the parent supercell). Small tick marks are plotted every 500 m. Note: if you are viewing this PDF file digitally, zoom in to increase legibility of vectors.

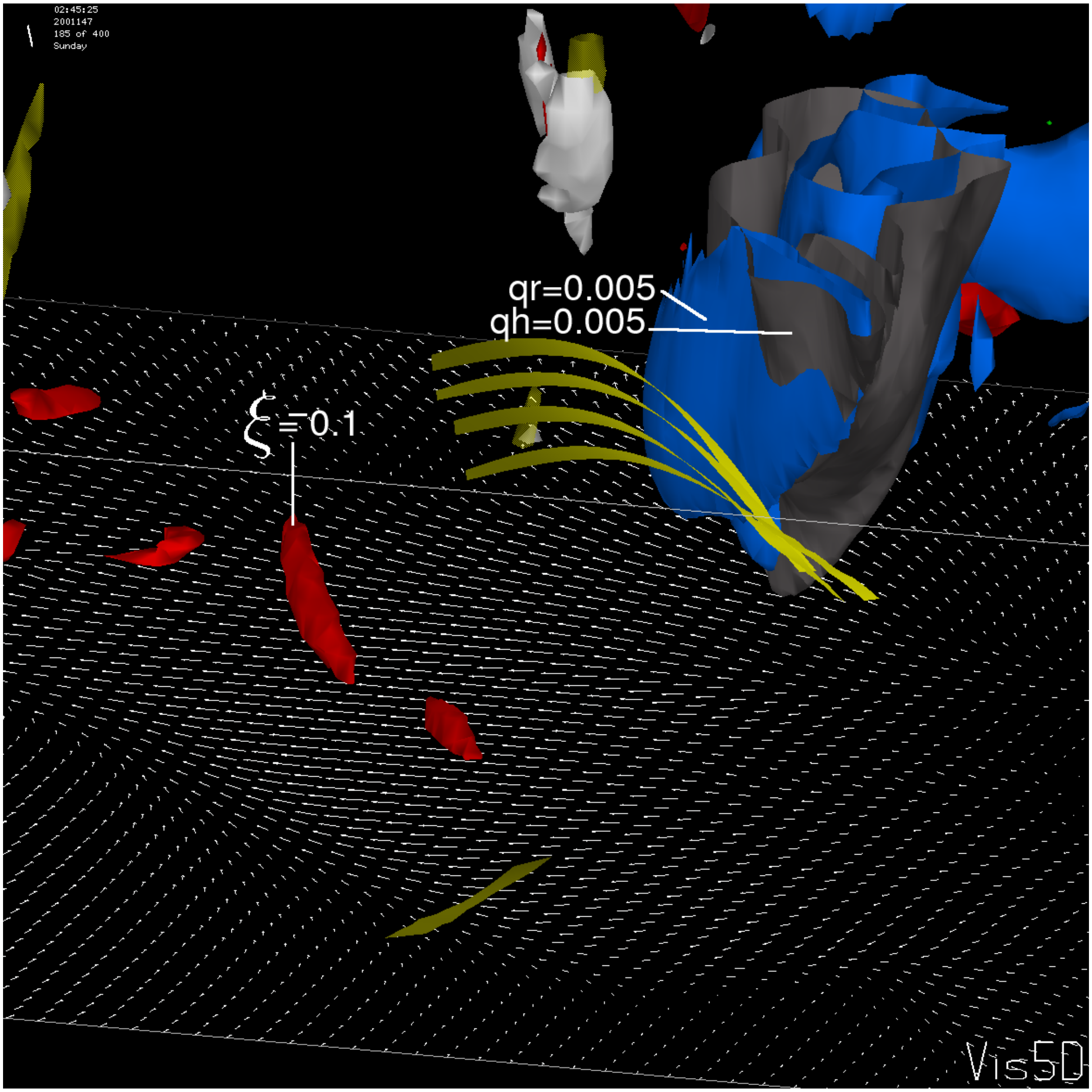

Figure 4: A view towards the WSW of the following isosurfaces: rainwater (0.005 kg/kg), hail (0.005 kg/kg), and ξ (-0.1 s^{-1}). Surface wind vectors and four trajectory ribbons are also shown. Model time is 2:45:25.

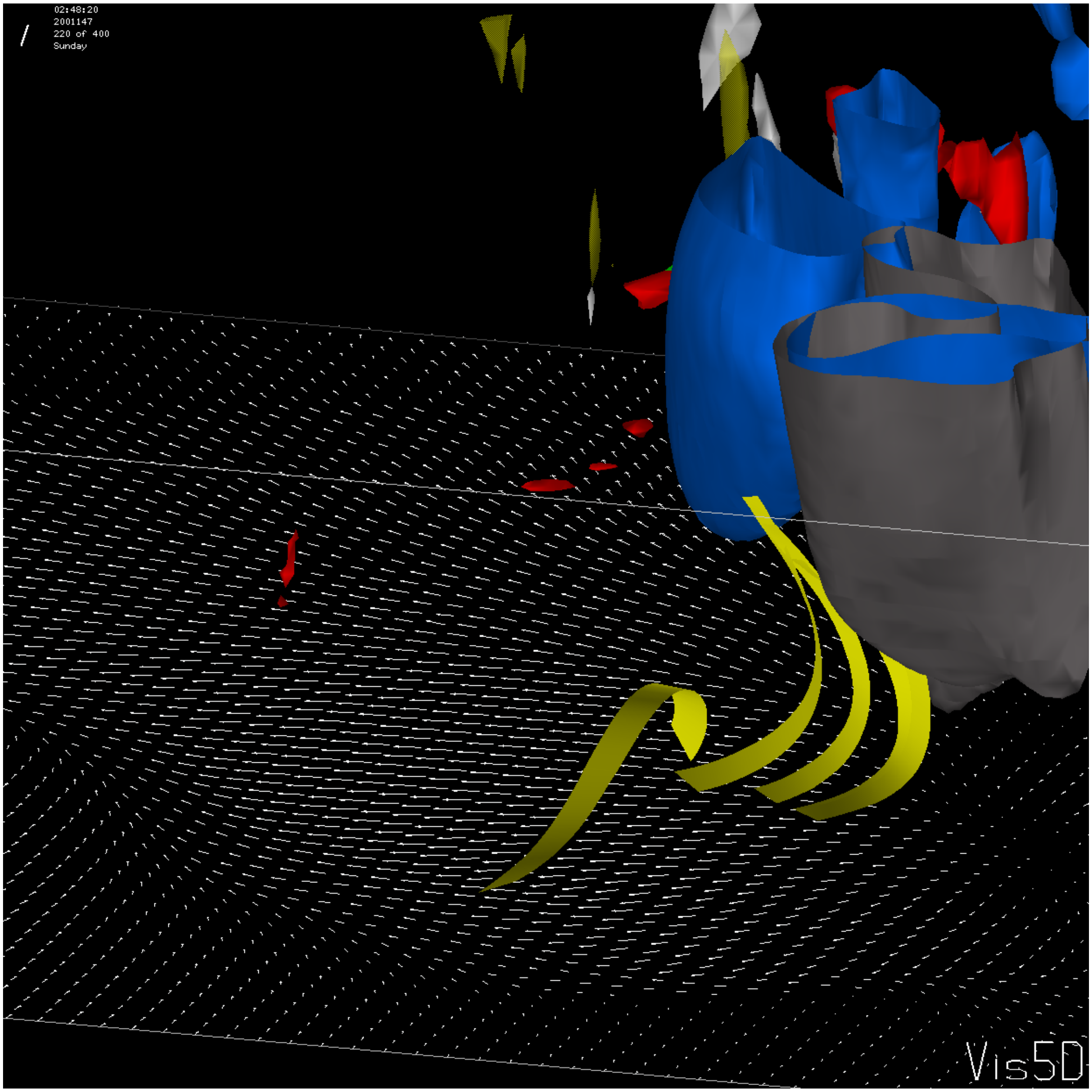

Figure 5: As in Fig. 4 at 2:48:20.

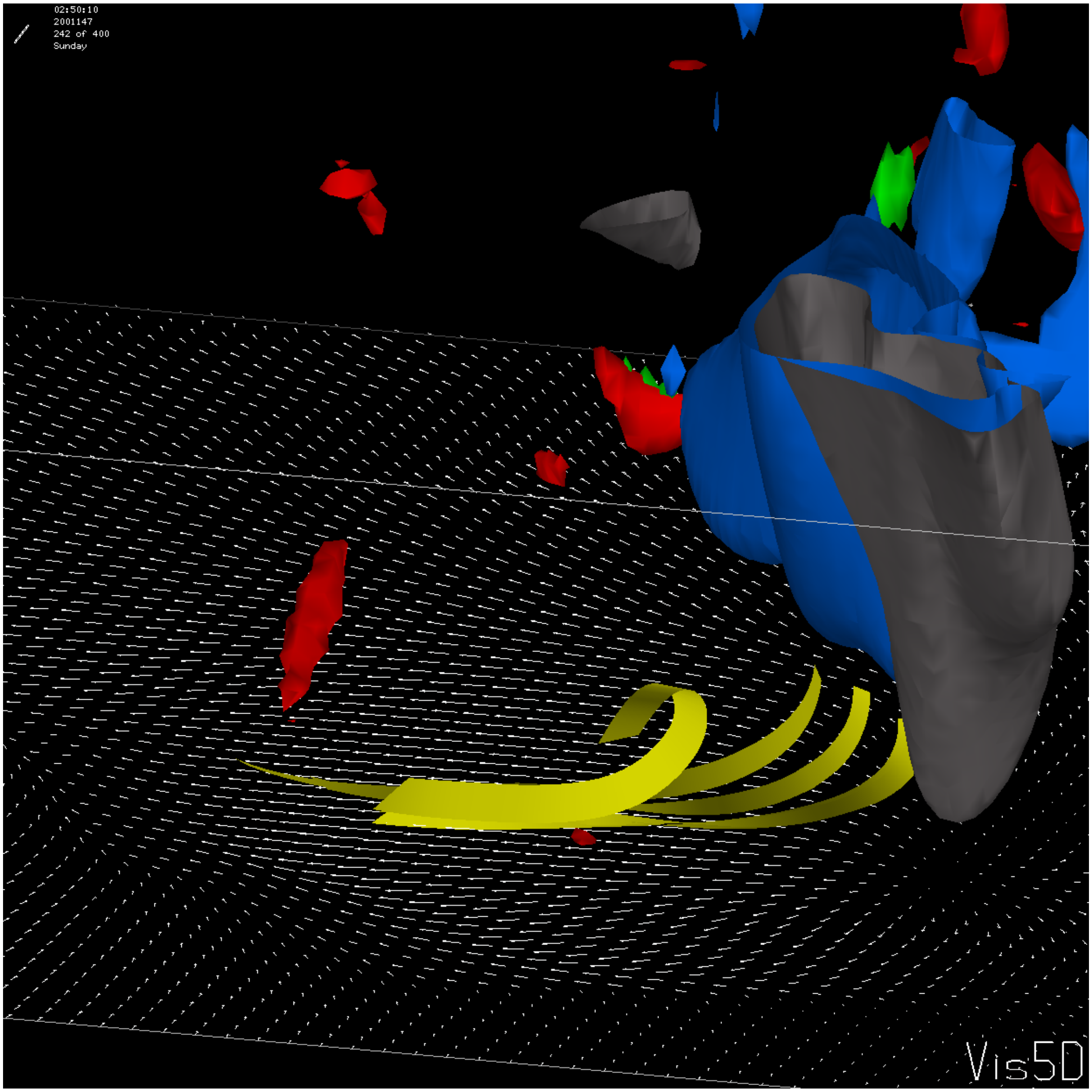

Figure 6: As in Fig. 4 at 2:50:10.

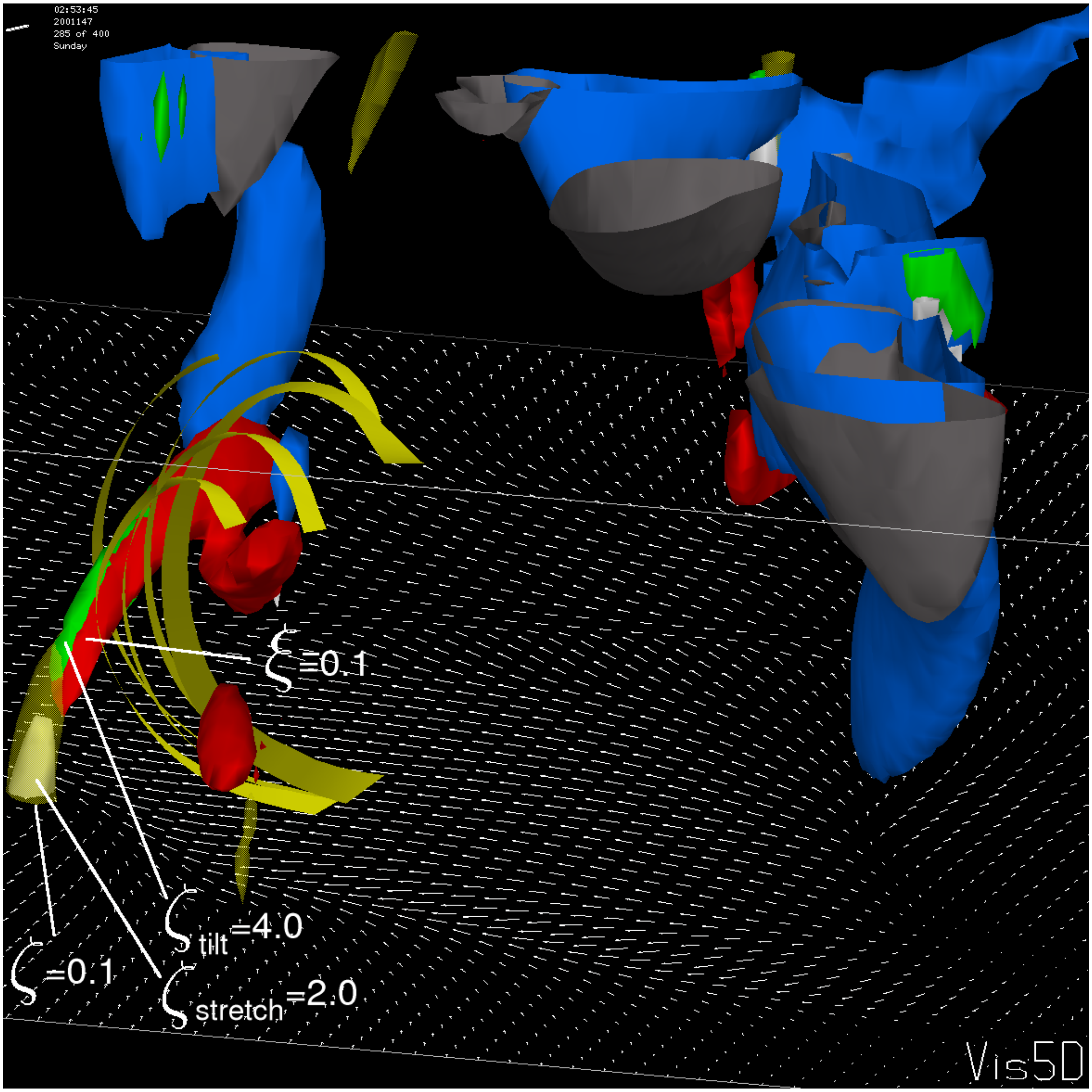

Figure 7: As in Fig. 4 at 2:53:45. The tilting (green) and stretching (white) terms of the vertical vorticity equation are shown (units of 10^{-4} s^{-2}), as well as ζ (transparent yellow isosurface, units of s^{-1}) and ξ.

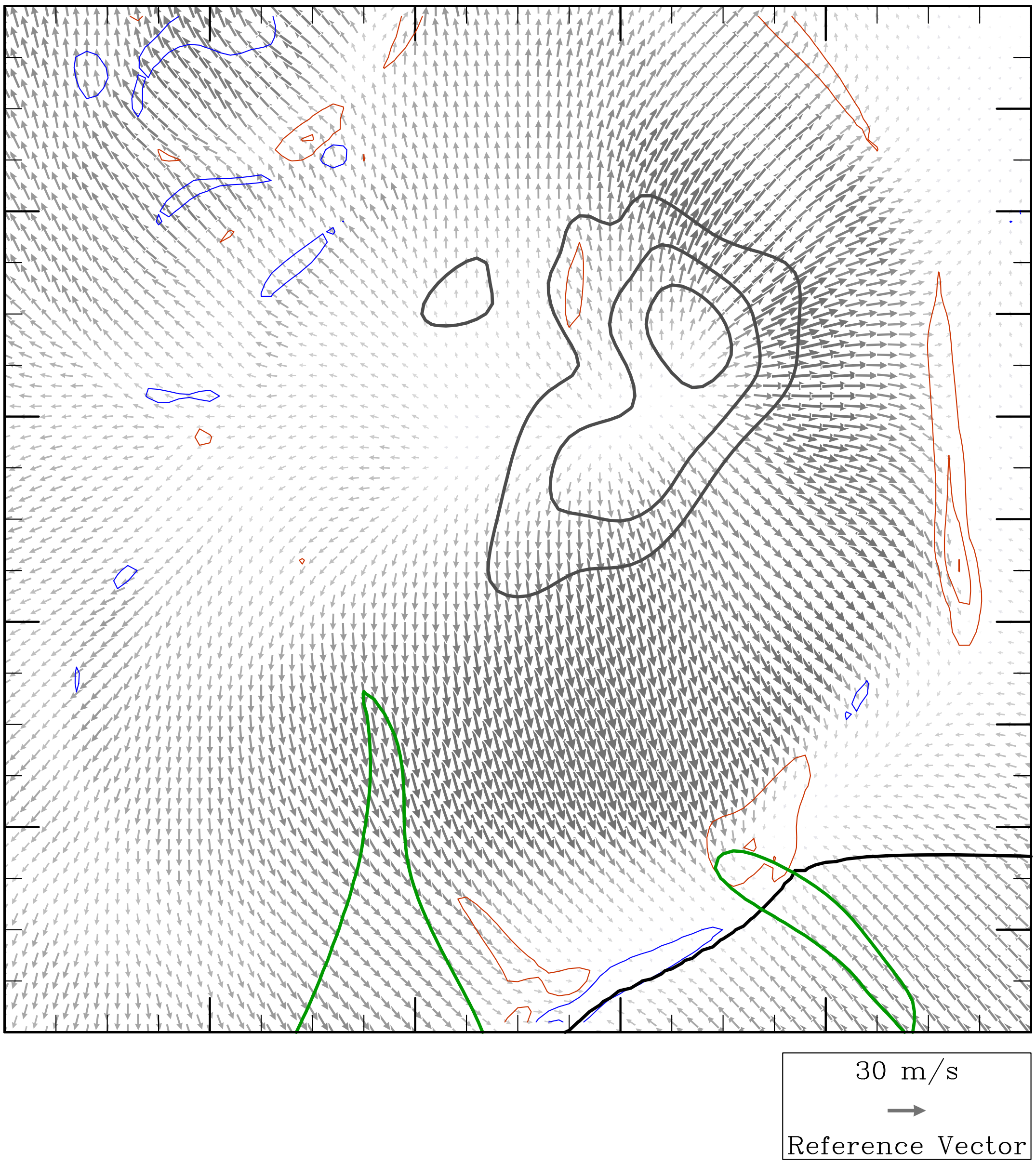

Figure 8: Contours of surface hail mixing ratio in 1 g kg^{-1} intervals at 2:50:45 (thick grey lines), updraft location at 2.7 km (20 m s^{-1} solid green contour), vertical vorticity in 0.03 s^{-1} intervals starting at +/- 0.01 s^{-1} (red/blue thin contours) and cold pool boundary (θ = 301.5 K). Storm-relative wind vectors are located every other model gridpoint for clarity. Small tick marks are plotted every 500 m.

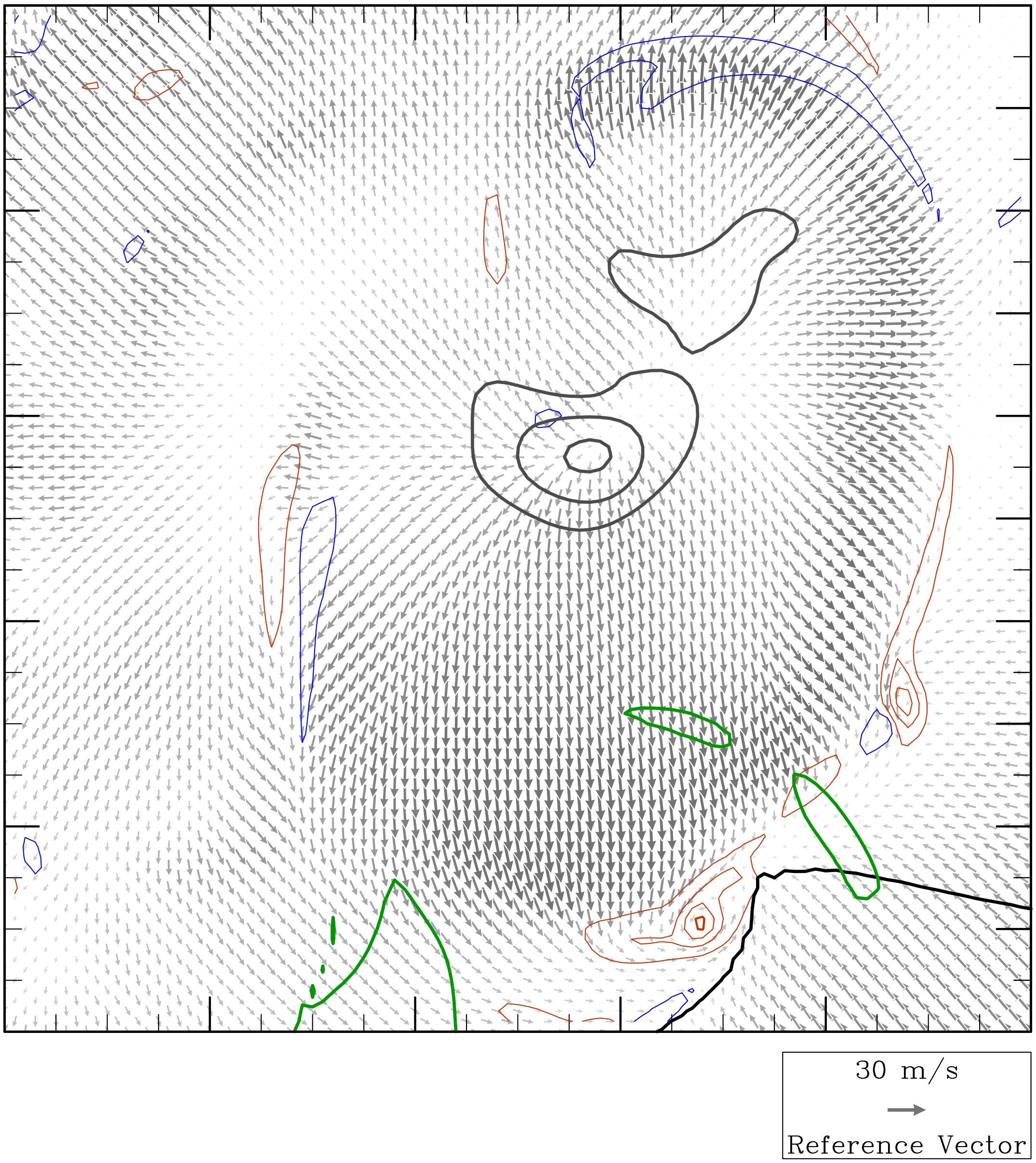

Figure 9: As in Fig. 8 at 2:52:35.

Figure 10: A view from the west of the updraft (red 30 m s^{-1} isosurface) and magnitude of the vorticity vector (gold 0.1 s^{-1} isosurface) at 2:59:35.